

NATIONAL INSTITUTE OF SCIENCE
EDUCATION AND RESEARCH

SIXTH SEMESTER PROJECT REPORT

**Study on spin Hall effect in
NM/HM bilayer & trilayer systems**

Author:

Ashish PANIGRAHI

Supervisor:

Dr. Kartik SENAPATI



*A report submitted in fulfillment of the requirements
for the course of P398*

in the

Superconducting Spintronics Lab
School of Physical Sciences

NATIONAL INSTITUTE OF SCIENCE EDUCATION AND RESEARCH

Abstract

Dr. Kartik Senapati

School of Physical Sciences

P398

Study on spin Hall effect in NM/HM bilayer & trilayer systems

by Ashish PANIGRAHI

Numerous studies on detecting spin current involve either using optical methods such as Kerr microscopy or electrical detection methods [1, 2] where spin current is generated beforehand and subsequent detection is done.

In contrast to these methods, we employ a rather simpler version by using electrical detection methods to measure spin current by a priori supplying an electric current with which we generate and measure the resultant spin current with a nano voltmeter.

Acknowledgement

I would like to take this opportunity to thank my supervisor, Dr. Kartik Senapati, for supervising me for my sixth semester project. His guidance and constructive feedback helped me in improving my work.

I would also like to especially thank my collaborator, Mr. Tapas Ranjan Senapati, who guided me in working with the instruments and made sure that I understood the relevant concepts required for the project.

Contents

Abstract	i
Acknowledgement	ii
1 Introduction	1
1.1 Spintronics: an emerging field	1
1.1.1 Why is spin current so important?	1
1.2 Aim and motivation behind the experiment	2
2 The Hall Effects	3
2.1 Introduction - Ordinary Hall effect	3
2.1.1 Mechanism of OHE	3
2.1.2 Hall coefficient	4
Calculating the Hall coefficient	5
2.2 Anomalous Hall effect (AHE)	7
2.2.1 Mechanism of AHE	8
2.3 Spin Hall effect (SHE)	8
2.3.1 Spin Current	9
2.4 Inverse Spin Hall effect (ISHE)	10
3 A semiclassical approach to SHE	11
3.1 SHE revisited: relation with AHE	11
3.1.1 Spin Hall Angle (SHA)	11
3.1.2 An overview of spin orbit interaction	12
Spin Orbit Coupling (SOC)	13
3.2 Mechanisms behind the phenomena	14
3.2.1 Extrinsic	14

3.2.2	Intrinsic	17
4	Methodology	18
4.1	Experimental plan	18
4.2	Preparation of sample	19
4.2.1	Fabrication of the sample	19
4.2.2	Motivation behind choosing Pt and Cu	19
4.3	Detecting spin current	20
Mathematical formulation of spin voltage	21	
Dependence of depth of slab on V_{SH}	23	
Extrapolation of V_{SC} via OHE	24	
4.4	Measurement	24
4.4.1	Efficacy of the measurement	24
4.4.2	Expected workflow	25
4.4.3	Final step	26
5	Results	27
5.0.1	Measurement via extrapolation in the presence of external B field	29
5.0.2	Inference	29
6	Limitations & future prospects	31
6.1	Conclusion	31
6.2	Limitations	31
6.2.1	Generation of spin imbalance in Pt	31
6.2.2	Poor conversion efficiency	32
6.2.3	Complications with multilayered systems	32
6.2.4	Thickness of layer	32
6.3	Scope for improvement	32
6.4	Future prospects	33

List of Figures

2.1	Schematic diagram of the Hall effect <i>Image courtesy: Ashcroft & Mermin, Solid State Physics</i>	4
2.2	A more "self-explanatory" diagram of the Hall effect <i>Image courtesy: C.M Hurd, The Hall effect in metals and alloys</i>	5
2.3	Schematic behaviour of the Hall resistivity ρ_H as a function of magnetic induction B in a metal showing appreciable magnetization. <i>Image courtesy: C.M Hurd, The Hall effect in metals and alloys.</i>	7
2.4	The total sum of rate of all charge variations across a surface is equal to the total current entering the surface. <i>Image courtesy: "Spin Current", Ken-ichi Uchida and Eiji Saitoh</i>	10
2.5	Comparison between SHE and ISHE. <i>Image courtesy: M.B Jungfleisch, PhD Thesis</i>	10
3.1	Relative motion of nucleus around the electron. <i>Image courtesy: Binghai Yan, "Spin-orbit coupling: A relativistic effect", Summer school on "Topological Matter States 2016"</i>	12
3.2	Extrinsic scattering mechanisms responsible for SHE: (c) skew-scattering and (d) side jump <i>Image courtesy: [16]</i>	14
3.3	Semiclassical picture of skew-scattering mechanism <i>Image courtesy: G. Vignale. "Ten Years of Spin Hall Effect".</i>	15
3.4	A semiclassical diagram of side-jump mechanism during a head-on collision with an impurity. <i>Image courtesy: G. Vignale. "Ten Years of Spin Hall Effect".</i>	16
4.1	Side view of the trilayer sample	19
4.2	Patterned Cu/Pt sample used in the experimental setup.	20
4.3	Schematic diagram depicting method to measurement of spin current. <i>Image courtesy: JE Hirsch. "Spin Hall effect" Phys. rev. letters (1999)</i>	21
4.4	Schematic diagram of the setup (<i>Blue represents the H-structure</i>). Pure charge current is supplied across the left arm and the potential difference is measured across the right arm of the sample.	25
4.5	A schematic representation of the workflow of the experiment.	26
5.1	Variation of voltage as a function of temperature at constant input current.	27

5.2	Variation of voltage for a range of temperature ($\approx 2 K$ to $10 K$ at constant currents $1 \mu A$ and $500 \mu A$)	28
5.3	Testing voltage as a function of temperature against background.	29
5.4	At $T = 2 K$, variation of potential difference as input current is varied from $-2 mA$ to $+2 mA$ for a finite number of runs.	30
5.5	Plot of voltage V vs external magnetic field B , in presence of an external magnetic field	30

List of Abbreviations

OHE	Ordinary Hall Effect
AHE	Anomalous Hall Effect
SHE	Spin Hall Effect
ISHE	Inverse Spin Hall Effect
NM	Normal Metal
HM	Heavy Metal
SOC	Spin Orbit Coupling
SHA	Spin Hall Angle

Chapter 1

Introduction

1.1 Spintronics: an emerging field

Spintronics is an emerging field in the technological sphere, which aims to complement the traditional role of electrons as charge carriers and exploit its properties related to spin. Conventionally, all electronic devices use binary digits 0 and 1 for store information in the form of the electron's charge. All such devices operate on components called transistors which are responsible for the flow of electric current to facilitate the processing of information.

Moore's law predicts that the number of transistors on such devices doubles every eighteen months [3]. However, this consequently also means that the size of individual transistors decreases. This raises a problem as the size of the transistors decrease, quantum phenomena become more dominant at such length scales. This difficulty is compensated by the rise of spintronics, which is seen as an alternative technology, based on the spin of the electron along with its charge to store and carry information.

The evolving field has its future prospects in making energy efficient devices with high storage density and low power consumption [4].

1.1.1 Why is spin current so important?

Pure spin current refers to the flow of a net angular momentum where there is no measurable charge current (the type of current that we can measure using ammeters) and plays a crucial role in the field of spintronics.

Conventional devices are based on the charge of the electron and do not depend on its spin. However, newer devices are being built that exploit this very property [5, 6]. Such devices would require low power to operate and have much faster switching times (switching 0s to 1s and vice versa) than conventional devices, simply because manipulating spin is much faster and costs less power.

1.2 Aim and motivation behind the experiment

Past studies have demonstrated that it is possible to detect spin current via a one-way conversion pathway involving spin Hall effect and to be able to use magneto-optical detection techniques to measure spin current [1, 2].

In contrast to the above however, in our experiment we intend to use conventional electrical detection techniques to measure spin current (refer section 2.3.1) directly using charge current as our input to the bilayer sample. This involves a two-way conversion pathway as opposed to the former method, but provides the opportunity for more simpler means of measurement.

In our study, we present the intricacies and results yielded from the experiment along with the difficulties faced and scope for improvement for the experiment.

Chapter 2

The Hall Effects

2.1 Introduction - Ordinary Hall effect

These effects originally deal with the application of an external magnetic field on a current carrying material and subsequently observing the effect either on the conductor or the electric current itself.

In 1879, Edwin Hall was exploring this interaction and tried to determine the effect of the magnetic field on a current carrying wire, with a suspicion that it either affected the whole length of the wire or only the moving electrons.

He later devised a rather simple experiment based on the argument that “if the current of electricity in a fixed conductor is itself attracted by a magnet, the current should be drawn to one side of the wire, and therefore the resistance experienced should be increased.” [7]

Hall couldn’t detect this extra resistance (which we now know as magnetoresistance) but concluded that a transverse force in the opposite direction must exist and which appears as a transverse voltage across the width of the conducting material. This is the Hall effect and the transverse voltage is the Hall voltage.

The experiment by Hall is shown in fig. 2.1.

2.1.1 Mechanism of OHE

In the fig. 2.1 , an electric current is passed along the x direction with corresponding current density is j_x . The cause of this current is an external electric field along the same direction, E_x .

An external magnetic field H along the z direction is applied and the Hall effect is observed.

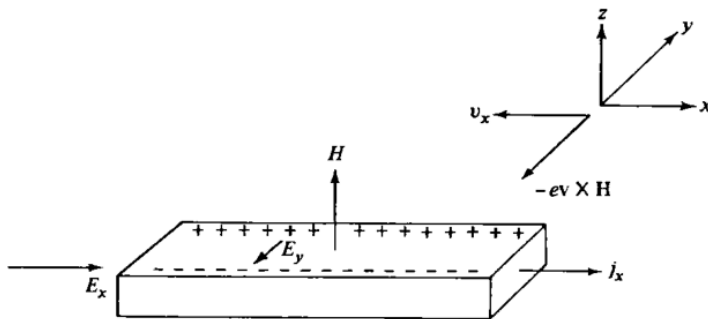


FIGURE 2.1: Schematic diagram of the Hall effect
Image courtesy: Ashcroft & Mermin, Solid State Physics

From the Lorentz force equation

$$\mathbf{F} = q(\mathbf{E} + \mathbf{v} \times \mathbf{H}) \quad (2.1)$$

The second term of the eq. (2.1) is responsible for deflecting the trajectory of the electrons in the negative y -direction and accumulating along the sides of the material. As this accumulation takes place, an electric field builds up along the y -direction which opposes the further deflection of electrons towards the sides. This process continues until an equilibrium is reached, at which this transverse field (or **Hall field**) E_y perfectly balances the Lorentz force and the current flows only along the longitudinal direction [8].

2.1.2 Hall coefficient

This transverse Hall field E_y can be thought of to be proportional to the external magnetic field H and longitudinal current density j_x . Here, we define the Hall coefficient as

$$R_H = \frac{E_y}{j_x H} \quad (2.2)$$

A rather interesting point to note is that by our construction, j_x and H are along positive x and z directions respectively. E_y however, is along negative y direction, meaning that the resultant sign of the Hall coefficient R_H is negative.

Now, imagine if the charge carriers were positive, this would result in their velocity along x -direction to get reversed (j_x would still be along positive x -direction). The Lorentz force would remain unchanged (as can be seen from eq. (2.1)). Consequentially, the direction of Hall field would be in the opposite direction compared to its direction in the case of negatively charged carriers.

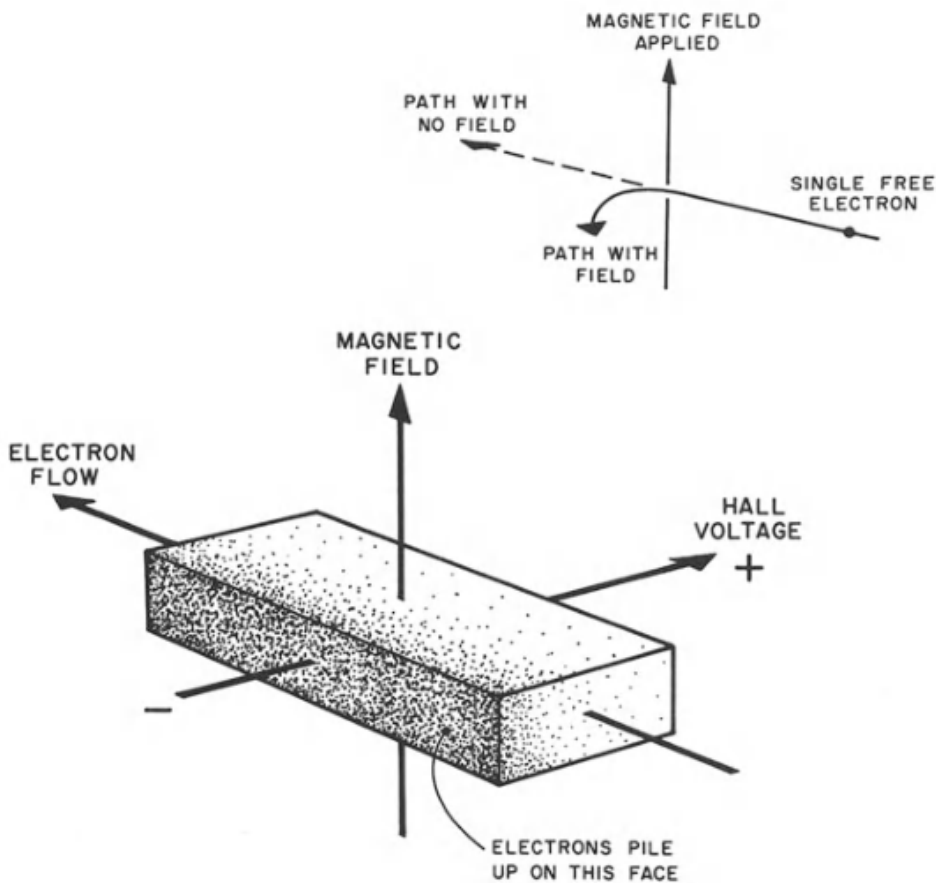


FIGURE 2.2: A more "self-explanatory" diagram of the Hall effect

Image courtesy: C.M Hurd, The Hall effect in metals and alloys

This would mean that measuring the Hall coefficient of a material, would help one determine the sign of the charge carriers [8].

Calculating the Hall coefficient

Let us consider current densities j_x and j_y in the presence of an electric field with components E_x and E_y , and in the presence of an external magnetic field H along the z -axis.

The average force per electron is given by the Lorentz force equation, i.e. $\mathbf{F} = -e(\mathbf{E} + \mathbf{v} \times \mathbf{H})$, and hence the average momentum per electron becomes

$$\frac{d\mathbf{p}}{dt} = -e \left(\mathbf{E} + \frac{\mathbf{p}}{m} \times \mathbf{H} \right) - \frac{\mathbf{p}}{\tau} \quad (2.3)$$

During equilibrium, the current becomes time-independent, and hence p_x and p_y satisfy the equations

$$\begin{aligned} 0 &= -eE_x - \omega_c p_y - \frac{p_x}{\tau} \\ 0 &= -eE_y + \omega_c p_x - \frac{p_y}{\tau} \end{aligned} \quad (2.4)$$

where

$$\omega_c = \frac{eH}{m} \quad (2.5)$$

Solving the above equations, we get

$$E_y = -\left(\frac{\omega_c \tau}{\sigma_0}\right) j_x = -\left(\frac{H}{ne}\right) j_x \quad (2.6)$$

This yields the Hall coefficient (eq. (2.2)) to be

$$R_H = -\frac{1}{ne} \quad (2.7)$$

where n is the number density of the charge carriers.

This is a rather astonishing result, suggesting that the Hall coefficient of a material, depends solely on the density of the carriers [8].

We then define Hall resistivity ρ_H as the Hall field E_y per unit longitudinal current density j_x , which is given by

$$\rho_H = \frac{E_H}{j_x} = R_H H \quad (2.8)$$

where the symbols have their usual meanings.

We shall stop our investigation on OHE in lieu of the main topic of the report.

2.2 Anomalous Hall effect (AHE)

The previous section dealt with OHE where the nature of the current carrying material is immaterial. Now, we deal with specific characteristics of such material, namely, magnetic metals.

It is observed that when observing Hall effect in such magnetic materials, in addition to OHE, certain unusual phenomena are observed.

In low-field conditions as seen from eq. (2.8), the observed Hall resistivity ρ_H varies linearly with external magnetic field H with the slope given by the Hall coefficient R_H . For illustration purposes, the example of Hall resistivity ρ_H has been used. The trend is the same for Hall field E_H as can be observed from eq. (2.8).

What about magnetic metals? In such materials, a linear but rapid rise in the Hall field is seen with increasing external magnetic field \mathbf{H} . This is followed by a secondary linear rise (with a lower gradient compared to the first), which later saturates at large fields and becomes almost independent of the external field. This is depicted in fig. 2.3

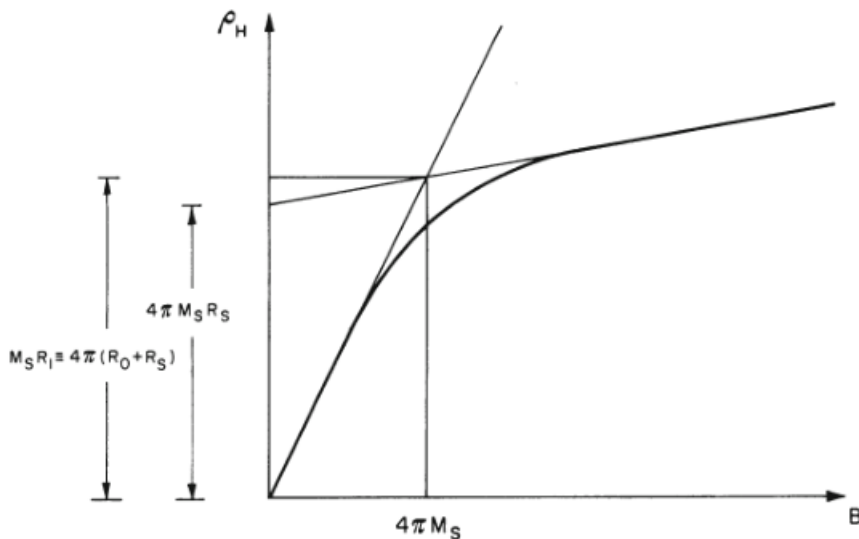


FIGURE 2.3: Schematic behaviour of the Hall resistivity ρ_H as a function of magnetic induction B in a metal showing appreciable magnetization.

Image courtesy: C.M Hurd, The Hall effect in metals and alloys.

In this case, the Hall effect is not simply from the application of Lorentz force on the charge carriers but rather seen as an *anomaly* and is therefore known as the **anomalous Hall effect**.

2.2.1 Mechanism of AHE

It has been shown empirically that this anomalous behaviour can be explained by a superposition of OHE and a strongly temperature dependent term. The curve shown in fig. 2.3 can be empirically fitted by the following equation (in CGS units):

$$\rho_H = R_0 B + \mu_0 R_s M \quad (2.9)$$

where B is the applied magnetic field, R_0 is the ordinary Hall coefficient, M is the magnetization of the material, R_s is the anomalous Hall coefficient and μ_0 is the permeability of free space.

The first term in eq. (2.9) accounts for OHE and is characterized by the more familiar eq. (2.8), whereas the second term is a characteristic of magnetic materials. This magnetization M can be present even without the presence of an external magnetic field \mathbf{B} , especially in ferromagnetic materials.

Especially in the case of ferromagnets, R_s is experimentally found to be strongly temperature dependent [9].

2.3 Spin Hall effect (SHE)

In this type of Hall effect, we generally deal with non-magnetic (or weakly magnetic) materials. For example, a paramagnetic material or a ferromagnetic material beyond its Curie temperature [10]. Strictly speaking, an external magnetic field is not *mandatory* to observed SHE.

When a charge current is supplied in a specific direction along a conducting material, an addition parameter of the charge carriers, namely, the spin of the electrons is responsible for this unique phenomena to take place.

For an electrical (charge) current flowing through a sample known to exhibit the phenomena¹, certain scattering mechanisms² preferentially scatter electrons in a direction perpendicular to the flow of charge current, such that electrons with opposite spins get accumulated along the edges of the sample, giving rise to a spin current [11, 10].

¹Such samples must have high spin-orbit coupling.

²We shall discuss the plausible mechanisms responsible for the spin Hall effect in greater detail in the forthcoming chapters.

This phenomena is very similar and analogous to OHE, the only difference being that instead of opposite charge accumulation on lateral sides, electrons with opposite spins get accumulated.

2.3.1 Spin Current

A pure spin current can be defined as the flow of electrons of spin \uparrow moving in one direction and electrons of the opposite spin i.e. \downarrow electrons moving along the opposite direction. This results in no net charge current (since rate of movement of electrons in opposing directions is the same) and a net flow of angular momentum [12].

From the continuity equation,

$$\nabla \mathbf{J} + \frac{\partial \rho}{\partial t} = 0 \quad (2.10)$$

where \mathbf{J} is the current density and ρ is the charge density.

This eq. (2.10) implies charge conservation law and helps us define the charge current [13].

Analogously, we can define the spin current density \mathbf{J}_s with reference to conservation of spin angular momentum. Considering that spin angular momentum is conserved, we can then define the corresponding continuity equation as

$$\nabla \mathbf{J}_s + \frac{\partial \mathbf{M}}{\partial t} = 0 \quad (2.11)$$

where \mathbf{M} is the magnetization (magnetic moment per unit volume) of the sample. The eq. (2.11) defines the spin current density \mathbf{j}_s [14].

In real solids for most of the cases, the conservation of spin angular momentum is a good approximation. However, in general, the conservation does not hold true due to spin relaxation (due to collisions with impurities in the solid, the spins of the electrons does not remain polarized) [14]. This gives rise to a modified version of eq. (2.11) as:

$$\nabla \mathbf{J}_s + \frac{\partial \mathbf{M}}{\partial t} = -\mathbf{T} \quad (2.12)$$

where \mathbf{T} is an indicator of the non-conservation of spin angular momentum (due to spin relaxation and spin generation) [14].

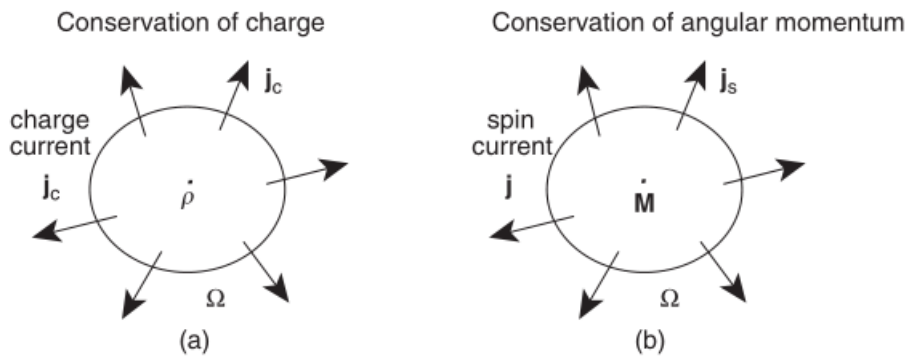


FIGURE 2.4: The total sum of rate of all charge variations across a surface is equal to the total current entering the surface.

Image courtesy: "Spin Current", Ken-ichi Uchida and Eiji Saitoh

2.4 Inverse Spin Hall effect (ISHE)

In contrast to SHE, the inverse Hall effect is essentially the same but SHE in reverse. When a pure spin current is injected into a material with high SOC (with no charge current), the same scattering mechanisms³ as the SHE, allow the spin-polarized electrons to preferentially scatter into opposite directions, leading to a charge imbalance across the edges of the material, thus resulting in a potential difference across the edges (in a transverse fashion) [15].

The spin \uparrow electrons scatter along one direction and the spin \downarrow electrons scatter along another direction. The surprising aspect about this, is that **both the directions are the same!** This leads to a pure charge current.

The fig. 2.5 is a schematic representation of the phenomena:

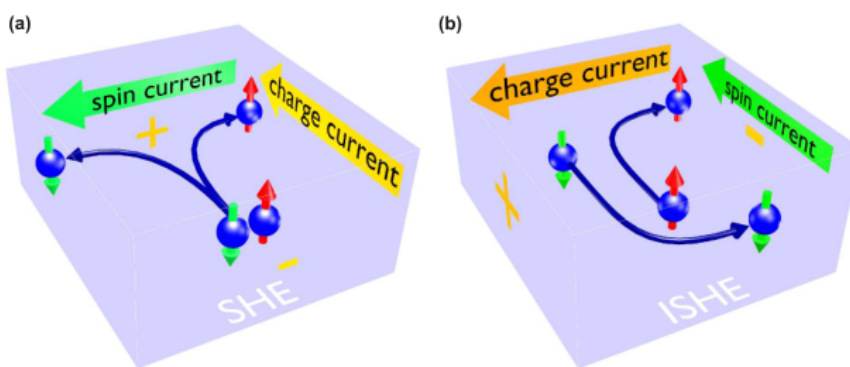


FIGURE 2.5: Comparison between SHE and ISHE.

Image courtesy: M.B Jungfleisch, PhD Thesis

³Discussed in detail in the next chapter.

Chapter 3

A semiclassical approach to SHE

In this chapter, we shall look at the semi-classical picture of SHE and try to understand the mechanisms behind the phenomena.

3.1 SHE revisited: relation with AHE

As seen in section 2.1, the OHE results in a charge imbalance along the edges of the conductor in the presence of an external magnetic field. We have also seen that in the case of SHE (sec 2.3), instead of a charge imbalance, we see a spin imbalance i.e. a preferential accumulation along the edges of the material.

Both AHE and SHE are similar in the way that there is a spin imbalance and hence an accumulation of carriers with opposite spins on opposite edges of the sample. The only difference is that in the case of AHE, there is a net magnetization of the material (since we typically use magnetic materials for AHE). This gives preferential scattering of the carriers based on spin but with unequal proportion i.e. due to the net magnetization of the material, the proportion of spin up \uparrow and spin down \downarrow is unequal and hence there will be disproportionate accumulation of one spin (\uparrow or \downarrow) from another (\downarrow or \uparrow).

A significant advantage of SHE over AHE is that the former doesn't require an external magnetic field to function. As long as the material in question possesses a high spin-orbit interaction, SHE is observed and the conversion of pure charge current (unpolarized electrons) gets converted into pure spin current (polarized electrons) with no charge current [10].

3.1.1 Spin Hall Angle (SHA)

A parameter of importance in the context of SHE, is the spin Hall angle θ_{SH} which is defined as

$$\theta_{SH} = \frac{\sigma_{xy}^s e}{\sigma_{xx}^c \hbar} \quad (3.1)$$

where σ_{xy}^s is the transverse conductivity due to spin current, σ_{xx}^c is the longitudinal conductivity due to charge current, and e is the charge of an electron.

θ_{SH} is the ratio of spin Hall conductivity to charge conductivity and quantifies the efficiency of conversion from charge to spin current and vice-versa.

3.1.2 An overview of spin orbit interaction

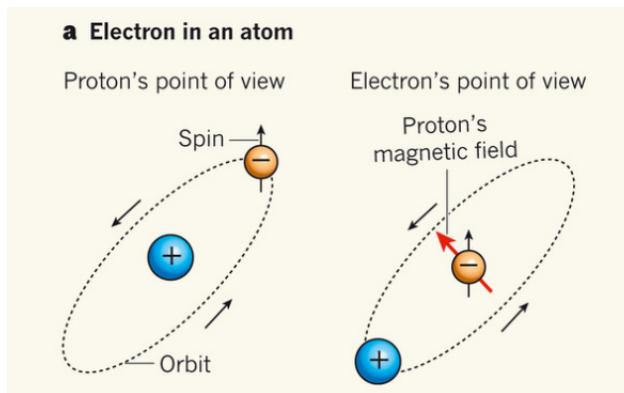


FIGURE 3.1: Relative motion of nucleus around the electron.

Image courtesy: Binghai Yan, “Spin-orbit coupling: A relativistic effect”, Summer school on “Topological Matter States 2016”

Consider a hydrogen atom where we take the electron’s frame of reference as depicted in fig. 3.1. In this frame, the positively charged nucleus (a single proton in this case) revolves around the electron. This induces a magnetic field¹ due to the moving proton, along the direction which is perpendicular to the plane of trajectory of the proton and whose magnitude is given by

$$B = \frac{\mu_0 I}{2r} \quad (3.2)$$

Each electron has an associated intrinsic spin, which induces a corresponding spin angular momentum. This spin also induces a spin magnetic dipole moment $\boldsymbol{\mu}_s$, which is given by:

$$\boldsymbol{\mu}_s = g_s \frac{e}{2m} \cdot \boldsymbol{S} \quad (3.3)$$

¹Equation (3.2) is easily derivable using Biot-Savart or Ampere’s law.

where g_s is the gyromagnetic ratio (≈ 2 for an electron) and \mathbf{S} is the spin angular momentum of the electron.

This presents the scenario where the magnetic dipole is in presence of an external magnetic field (due to the moving proton) and hence will feel a torque $\boldsymbol{\tau}$ which tries to align $\boldsymbol{\mu}_s$ in the direction of \mathbf{B} and is given by

$$\boldsymbol{\tau} = \boldsymbol{\mu}_s \times \mathbf{B} \quad (3.4)$$

This torque $\boldsymbol{\tau}$ will change the energy of the electron by an amount:

$$\Delta U = -\boldsymbol{\mu}_s \cdot \mathbf{B} \quad (3.5)$$

Spin Orbit Coupling (SOC)

Spin orbit coupling refers to the interaction between the spin angular momentum of electron and the orbital angular momentum of the atom.

Referring to fig. 3.1, the orbital angular momentum $\mathbf{L} = m\mathbf{r} \times \mathbf{v}$ of the atom is related to the magnetic field \mathbf{B} by

$$\mathbf{B} = \frac{\mu_0 Z e \mathbf{L}}{4\pi m_e r^3} \quad (3.6)$$

We see from eq. (3.6) and eq. (3.3) that

$$\boldsymbol{\mu}_s \propto \mathbf{S} \quad \text{and} \quad \mathbf{B} \propto \mathbf{L}$$

Applying the above relations in eq. (3.5), we get

$$\Delta U \propto \mathbf{S} \cdot \mathbf{L} \quad (3.7)$$

This means that orbital angular momentum of the nucleus and the spin angular momentum of the electron interact with each other, which results in the energy of the energy levels of the electrons in the atom. This is called the spin-orbit interaction.

3.2 Mechanisms behind the phenomena

Over the past century, the scientific community has agreed upon three plausible mechanisms responsible for SHE. These are categorized into extrinsic and intrinsic mechanisms. Let's dive into the details of the same.

3.2.1 Extrinsic

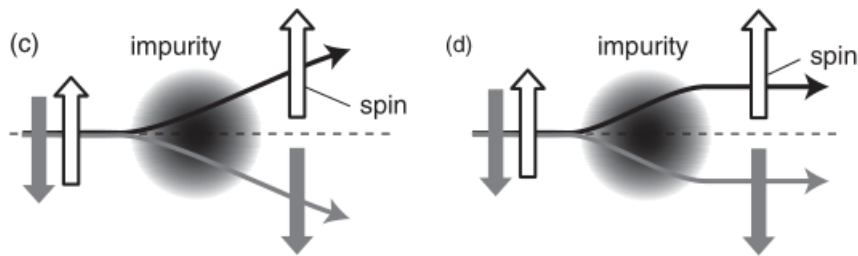


FIGURE 3.2: Extrinsic scattering mechanisms responsible for SHE: (c) skew-scattering and (d) side jump

Image courtesy: [16]

We know that for a material to exhibit SHE, spin-orbit interaction is required. One such origin of SOC is due to impurities in the sample, giving rise to "extrinsic" mechanisms of the forms:

1. Asymmetric scattering (skew-scattering)
2. Side-jump mechanism

Skew-scattering

Particles with intrinsic spin in the presence of SOC, are preferentially scattered by a central potential [17]. This central potential is due to the impurities in the sample.

Let us consider a case in two dimensions i.e. $x - y$ plane and that the impurities are spherically symmetric. In the presence of SOC, the impurities conserve orbital angular momentum L_z and spin angular momentum S_z separately. As the particles cross the vicinity of such impurities, the corresponding scattering cross-section depends on the relative sign of L_z and S_z along with the angle of scattering. For example, a greater ratio of spin \uparrow electrons will be scattered towards states of positive L_z (say) than towards states of negative L_z . This would result in more spin \uparrow electrons getting scattered to the left than to the right. A similar analogy but opposite in direction, is applicable for spin \downarrow electrons. The

direction of scattering also depends on the nature of interaction of the impurities i.e. if interaction between the impurity and electron is attractive or repulsive in nature.

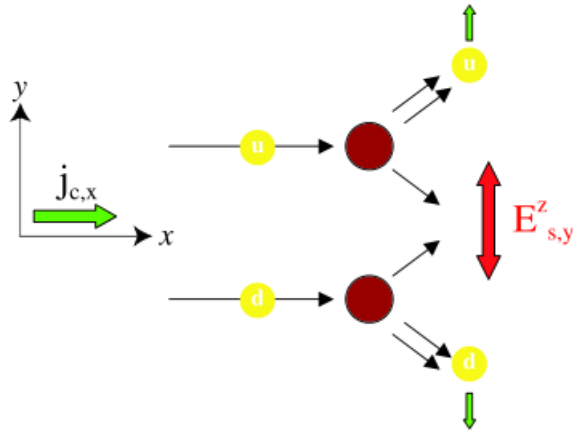


FIGURE 3.3: Semiclassical picture of skew-scattering mechanism

Image courtesy: G. Vignale. "Ten Years of Spin Hall Effect".

We proceed to calculate the contribution of skew-scattering towards SHE as described in [18].

Let us introduce a Fermi distribution along the direction of charge current $j_{c,x}$ where superscripts c and x denote pure charge current and direction of propagation respectively. An interesting analogy would be to consider an equivalent "spin electric field" $E_{s,y}$ (refer fig. 3.3) in the transverse direction which essentially pushes electrons in the y direction, with corresponding resistivity given as

$$\rho_{ss} = \frac{m^*}{ne^2\tau_{ss}}$$

where n is the electron number density, and τ_{ss}^{-1} is the skew scattering rate. This gives us the relation between the "spin electric field" and longitudinal charge current density as

$$E_{s,y} = \rho_{ss} j_{c,x} \quad (3.8)$$

The spin electric field is responsible for spin current along the transverse direction, which is related by the linear relation,

$$j_{s,y} = \sigma_s E_{s,y} \quad (3.9)$$

where σ_s is the spin conductivity and $j_{s,y}$ is the corresponding spin current density in the y direction.

Using simple Drude model, we also relate the longitudinal charge current density $j_{c,x}$ and longitudinal conductivity σ_c by the relation

$$j_{c,x} = \sigma_c E_x \quad (3.10)$$

where E_x is the corresponding electric field along x direction.

Multiplying equations 3.8, 3.9 and 3.10, and further cancelling common terms, we get contribution to SHE via skew-scattering as

$$\boxed{\frac{j_{s,y}}{E_x} = \sigma_{ss}^{SHE} \equiv \sigma_s \rho_{ss} \sigma_c} \quad (3.11)$$

Side-jump

Similar to skew-scattering, this mechanism is extrinsic in nature and depends on the spin-orbit interaction with the impurities.

However in contrast to skew-scattering, as seen from the schematic diagram in fig. 3.2, in this mechanism, there is a shift in the transverse component of velocity of the electrons, which arises from considering the electron as a wave packet (see fig. 3.4) with the collision, leading to an instantaneous change in the average momentum of the wave packet [19].

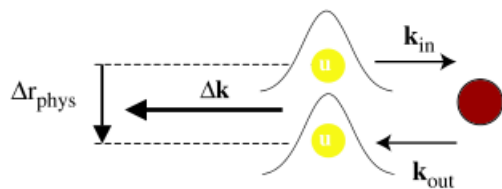


FIGURE 3.4: A semiclassical diagram of side-jump mechanism during a head-on collision with an impurity.

Image courtesy: G. Vignale. "Ten Years of Spin Hall Effect".

We shall not dive into the mathematical details of the mechanism for the sake of brevity.

3.2.2 Intrinsic

As opposed to the extrinsic mechanisms described in earlier sections, the intrinsic mechanisms cause spin-dependent transverse scattering to occur due to the spin orbit interaction with the electronic band structure of the material.

In the case of extrinsic mechanisms, a gain in transverse velocity is observed *during* the scattering events. Meanwhile, in the case of intrinsic mechanisms, the transverse velocity gain is seen *between* the scattering events [20].

We shall not go over the mathematical intricacies of the mechanism for the sake of brevity.

Chapter 4

Methodology

In this chapter, we discuss about the techniques and methods used to devise an experiment involving a Pt-Cu bilayer system and subsequently investigate the effect of spin current via SHE.

4.1 Experimental plan

In earlier studies, it has been shown that a pure spin current can be generated and manipulated via a heavy metal through SHE [10, 21, 22]. The detection of this spin current can only be done via conversion into charge current (which is measurable) using ISHE. This generally involves a ferromagnetic layer or a magneto-optical method [23, 24, 25, 2].

In our study, we intend to explore the detection of spin current in a NM/HM trilayer system without a magnetic layer, i.e. via electrical means such as using a simple voltmeter.

In many studies involving the electrical detection of spin current, pure spin current is generated using a ferromagnet at one end of the sample structure, which then gets converted to charge current via ISHE, and is subsequently, detectable using a voltmeter at the other end of the structure (which is usually a non-magnetic metal with high spin-orbit coupling).

Contrary to the above method, we do not generate pure spin current beforehand, but rather provide a pure charge current as supply to our sample, which is converted to spin current via SHE and is converted back to charge current via ISHE. Keeping this in mind, we design our sample accordingly.

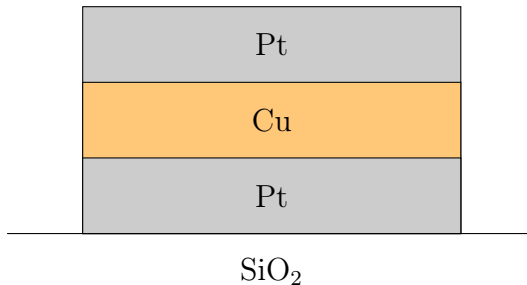


FIGURE 4.1: Side view of the trilayer sample

4.2 Preparation of sample

We prepare a trilayer system, using copper (Cu) as the NM and platinum (Pt) as the HM. Here, we sandwich a layer of Cu between two layers of Pt. This is depicted in fig. 4.1.

Now, as mentioned in section 4.1, we intend to make the shape of our sample to facilitate the conversion to charge to spin current and vice versa. As seen in section 2.4 we see that converted spin current, flows perpendicular to the original charge current and similarly during the back conversion via ISHE. For this, an obvious structural shape would be a path that has two paths, connected via a link being perpendicular to both the paths simultaneously. Hence, a H-like structure comes to mind, which is implemented in our experimental setup.

4.2.1 Fabrication of the sample

Using the techniques of photolithography¹, magnetron sputtering¹ and focused ion beam¹, we fabricate our sample as depicted in fig. 4.2.

4.2.2 Motivation behind choosing Pt and Cu

One might wonder, why specifically did we choose Pt and Cu as our bilayer/trilayer sample? We present the following reasons for choosing so:

- In a lot of experiments involving SHE [26, 27, 28, 29], Pt is used extensively due to its high spin Hall angle, which results from its high SOC. It also has good conductivity and is easy to grow onto thin films.
- Cu is used mainly because of its high spin diffusion length [30]. This allows spin polarized electrons to maintain coherence for longer length scales.

¹Details about these methods have been skipped for the sake of brevity.

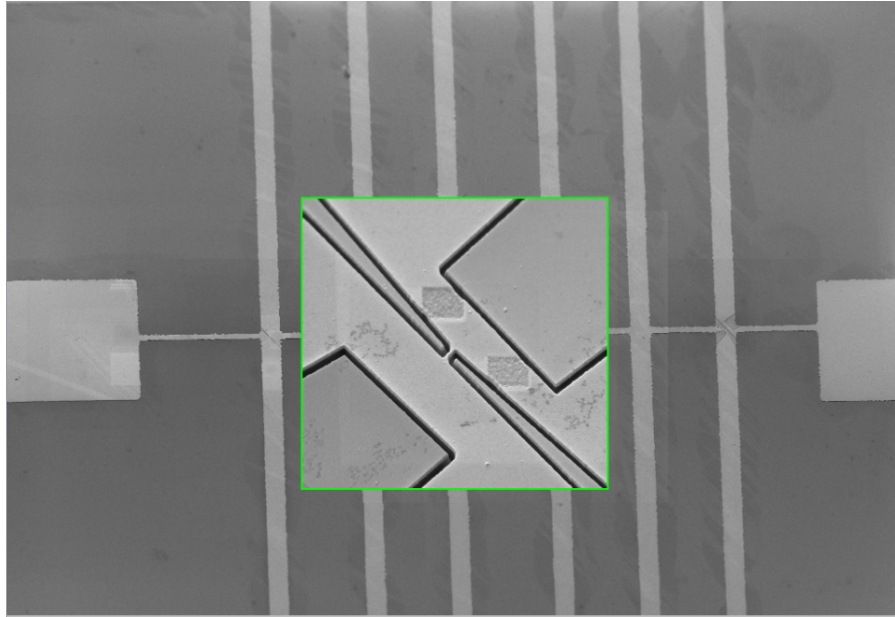


FIGURE 4.2: Patterned Cu/Pt sample used in the experimental setup.

4.3 Detecting spin current

In the case of OHE, the charge imbalance across the edges of the slab results in a potential difference (Hall voltage) V_H across the width of the sample. This voltage can then simply be measured using a voltmeter. But in the case of SHE, how does one go about measuring spin imbalance? In such a case, there is no net charge transfer and hence conventional electrical measurements cannot be used directly.

One plausible way would be to use an instrument to measure the difference in localized magnetization across the width of the slab. This can be achieved by using a superconducting quantum interference device microscope [31] to measure local magnetic fields; the details into which we shall not go over for the sake of brevity. A potential difficulty that arises in this approach would be to eliminate the contribution of magnetic field due to the longitudinal current density j_x , it being greater in magnitude would mask the magnetization along the edges due to spin polarized electrons [10].

We proceed to highlight a clever method to measure the spin current in a sample as proposed in [10].

The same scattering mechanisms (refer section 3.2) responsible for the conversion of charge current to spin current in the first place, will also be responsible for the conversion in the reverse direction i.e. ISHE. This fact is exploited and we argue that by connecting a transverse strip across the slab would allow spin current to flow through it (as seen in fig. 4.3).

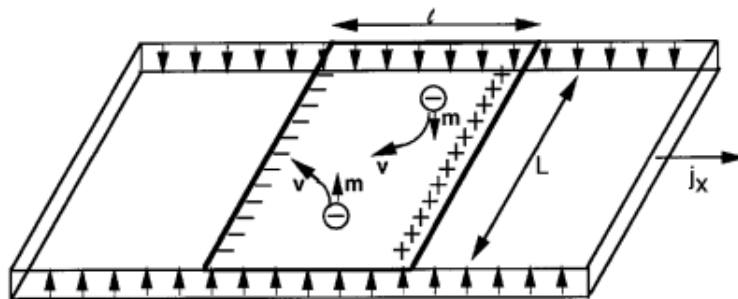


FIGURE 4.3: Schematic diagram depicting method to measurement of spin current.

Image courtesy: JE Hirsch. "Spin Hall effect" Phys. rev. letters (1999)

We take this strip made of a material (metal) with high SOC, only then can one observe ISHE to convert spin polarized electrons to a charge imbalance across width of strip. Let charge current density j_x travel along the longitudinal direction. The width of the slab is L and the width of the transverse strip is l . It is a necessary point to note that the width L cannot be more than the spin diffusion length δ_s of the material of the slab. δ_s is the maximum length of a material, upto which spin coherence of spin polarized electrons is maintained. Scattering mechanisms responsible for the phenomena, also lead to a loss of this spin coherence across a length scale given by δ_s , which is an intrinsic property of the material used.

As seen in the figure, charge current corresponding to j_x results in a spin imbalance across the edges of the slab due to SHE. This results in spin current².

This spin current moves in a perpendicular direction compared to j_x but in the plane of the slab. Via the same scattering mechanisms, the spin polarized electrons get preferentially scattered depending on the direction of their spins, resulting in a charge imbalance which is seen along the edges of the tranverse metal strip. This charge imbalance gives rise to a potential difference across the strip, which can be measured by conventional electrical instruments such as a voltmeter.

Mathematical formulation of spin voltage

The magnetization of a sample with n_{\downarrow} as the number density of spin polarized (spin down) electrons is given by

$$M = n_{\downarrow} \mu_B \quad (4.1)$$

²Described in the preliminary sections (refer section 2.3)

where $\mu_B = \frac{e\hbar}{2m_e}$ is the Bohr magneton.

Along with the longitudinal current density j_x , we get an anomalous Hall voltage across the width of the sample as

$$V_H = 4R_s L j_x n_{\downarrow} \mu_B \quad (4.2)$$

where R_s is the anomalous Hall coefficient and L is the transverse width of the slab.

Equation (4.2) can be extended for non-magnetic materials with high SOC, where the number density of spin \downarrow and spin \uparrow electrons is equal, giving rise to a “spin Hall voltage” V_{SH} , whose sign depends on the direction of spin of the electrons. This gives us the corresponding expression as,

$$V_{SH} = 2\pi R_s L j_x n \mu_B \quad (4.3)$$

where n is the total number density of conduction electrons and the rest of symbols have their usual meanings.

As described earlier, on connecting the edges of the slab via a transverse strip of metal, the spin imbalance will cause a spin current to propagate in the metal strip. The expression for spin current density is then written as

$$j_{\eta} = \frac{V_{SH}}{\rho L} \quad (4.4)$$

where η is an index for each spin, ρ is the resistivity of the transverse strip.

As the spin current propagates through the strip, the spin polarized electrons get preferentially scattered via ISHE, leading to a charge imbalance across the strip. This leads to a potential difference given by

$$V_{SH}^{\eta} = 4\pi R_s l j_{\eta} n_{\eta} \mu_B \quad (4.5)$$

where l is the width of the strip, j_{η} is the spin current density due to spin index η , n_{η} is the number density of electrons with spin index η .

Substitution of eq. (4.4) in eq. (4.5), gives us the expression for voltage due to spin current, which can be measured using a simple voltmeter:

$$V_{SC} = 8\pi^2 R_s^2 l \frac{(n\mu_B)^2}{\rho} j_x \quad (4.6)$$

Notice that in the above expression does not depend on the transverse width L anymore. However, there is an implicit dependence on L . This is presented in the fact that if L is comparable to the spin diffusion length δ_s of the slab, V_{SC} will decrease.

Dependence of depth of slab on V_{SH}

Let us analyze the dependence of width L of slab on V_{SH} from eq. (4.3). From the expression, the experimental parameters are L and longitudinal current density j_x . Let d be the depth of the slab and I_x be the charge current corresponding to j_x . Then, these quantities can be related as

$$j_x = \frac{I_x}{Ld}$$

Substituting this value for j_x in eq. (4.3),

$$\begin{aligned} V_{SH} &= 2\pi R_s L n \mu_B \left(\frac{I_x}{Ld} \right) \\ &= 2\pi R_s n \mu_B \left(\frac{I_x}{d} \right) \end{aligned} \quad (4.7)$$

Keeping the electrical current I_x constant throughout and taking $k = 2\pi R_s n \mu_B I_x$ as a constant, we rewrite eq. (4.7) as

$$V_{SH} = \frac{k}{d} \implies \boxed{V_{SH} \propto \frac{1}{d}} \quad (4.8)$$

We see that the spin Hall voltage is inversely proportional to the depth of the sample used. Therefore, to make a significant measurement, we require a thin slab.

Extrapolation of V_{SC} via OHE

In experiments involving the detection of spin current, an external magnetic field is not necessarily required but can be cleverly used. Consider the case where an external magnetic field is supplied along the direction perpendicular to the plane of the slab in addition to fig. 4.3.

We know for a fact that due to OHE, a Hall voltage will be induced across the edges of the slab, which consequently results in a charge current along the transverse strip, giving an additional part to the spin voltage in eq. (4.6). This total voltage is then given by [10] as

$$V_t(B) = (R_0^2 B^2 + R_s^2 B_{eq}^2) \frac{l}{\rho} j_x \quad (4.9)$$

where $B_{eq} = 4\pi n \mu_B / \sqrt{2}$, R_0 is the ordinary Hall coefficient and other symbols denote their usual meaning.

From an experimental perspective, it can be quite difficult to measure the spin current using this method, simply because the value of spin voltage is quite low for conventional voltmeters to be able to detect with significant precision.

To avoid this, an extrapolation technique involving OHE can be used, and is done as follows: voltage measurements in the presence of an external magnetic field is done (given by eq. (4.9)). The data obtained can then be extrapolated to points where $B = 0$, which effectively reduces to the original scenario of measuring spin current without involving OHE.

4.4 Measurement

After the sample is prepared, we pass electrical (pure charge) current through one arm of the H -structure and make voltage measurements across the opposite ends of the sample, as shown in fig. 4.4. This is technically called a non-local measurement.

4.4.1 Efficacy of the measurement

As seen in section 3.1.1, the efficiency of conversion of spin current to charge current and vice versa is related to the spin Hall angle of the material. However, this efficiency is very poor in practical laboratory environments. Earlier studies in measuring spin current [2], involved using a ferromagnetic layer to generate

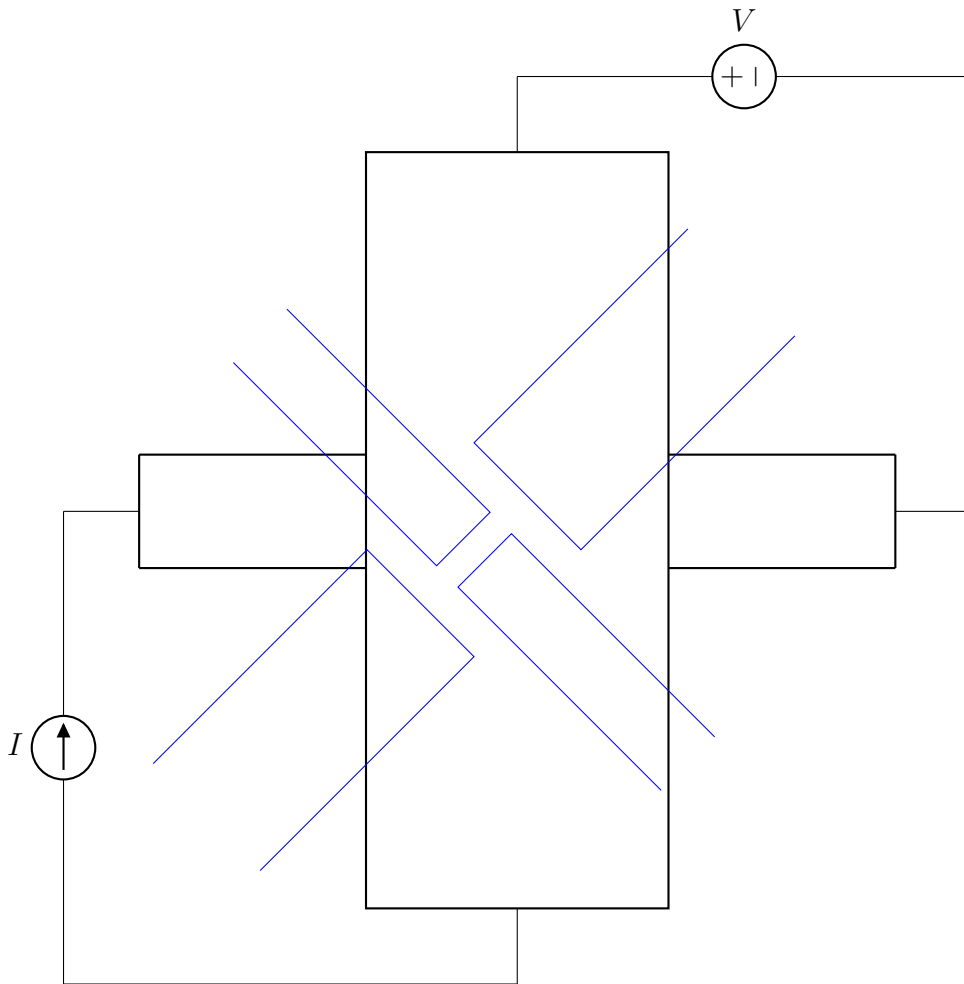


FIGURE 4.4: Schematic diagram of the setup (*Blue represents the H-structure*). Pure charge current is supplied across the left arm and the potential difference is measured across the right arm of the sample.

the spin polarized electrons, giving rise to spin current which is converted to charge current further down the experiment via ISHE. In these studies, the conversion occurs only once, in contrast to our study where we do this to-and-fro conversion **twice**, meaning that the efficacy of measuring the spin current is much less as compared to traditional approaches [2].

4.4.2 Expected workflow

As shown in fig. 4.5, we provide an input current density J_c , along one arm of the H-structure.

Referring back to fig. 4.1, we see that the middle layer is Cu, sandwiched between two Pt layers at one end of the H-structure.

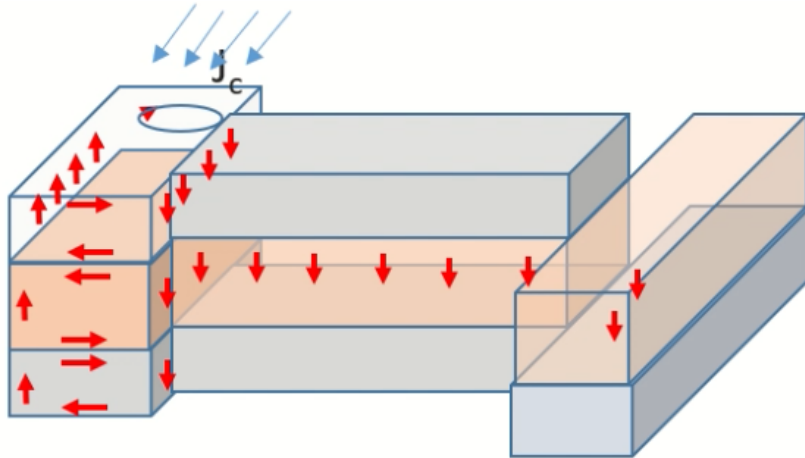


FIGURE 4.5: A schematic representation of the workflow of the experiment.

We now proceed to describe, the step-by-step process of the expected phenomena:

1. Input charge current density J_c moves through the first arm of the H-structure.
2. Due to high SOC of Pt (the two outer layers), spin imbalance is observed along the edges of the Pt layers (via SHE), and since the two layers are in close proximity, these spin polarized electrons move into the Cu layer.
3. Cu being a good conductor and having high spin diffusion length (about 500 nm at room temperature [32]), allows the spin current to propagate across the length of the arm-link layer, maintaining its spin.
4. At the other end of the H-structure, charge imbalance is generated via ISHE, which then leads to a potential difference on the right arm (as seen in fig. 4.5), which we measure non-locally using a voltmeter.

4.4.3 Final step

After making the measurement of potential difference via voltmeter, the measurement readings are analyzed.³

³Done in the following chapter.

Chapter 5

Results

We make the following measurements at varying:

- thickness of Pt and Cu layers; (10 nm, 20 nm, . . .)
- length and width of arm of the H-structure.

After making the aforementioned measurements, we proceed to analyze the resultant data.

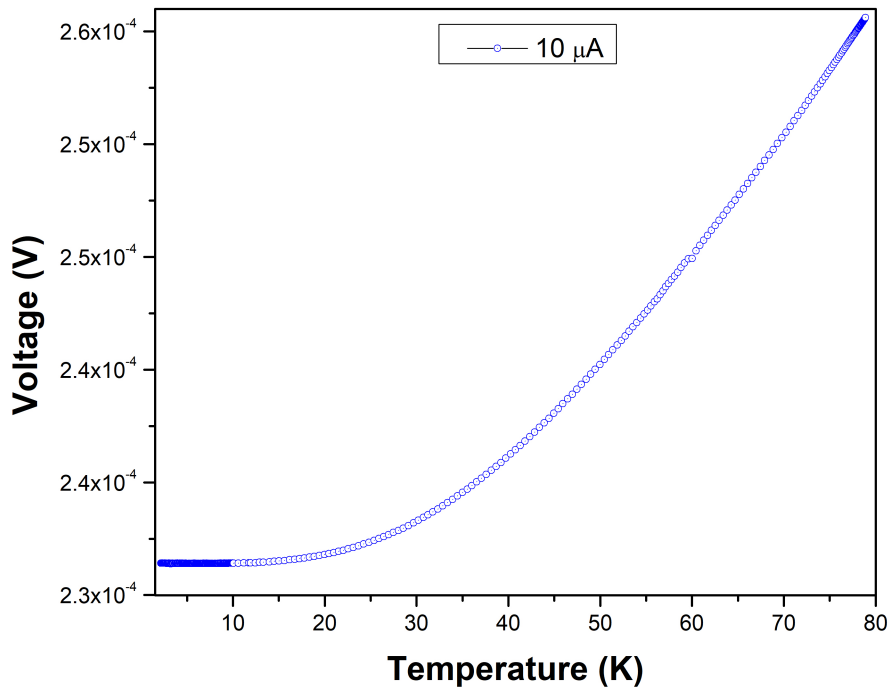


FIGURE 5.1: Variation of voltage as a function of temperature at constant input current.

Before the experiment is begun, we test if the sample track works as expected. We supply a fixed value of input current and make voltage measurements at various temperatures of the sample. As expected, we end up with a *voltage-vs-temperature* curve which is characteristic to that of a metal (Cu/Pt) (see fig. 5.1).

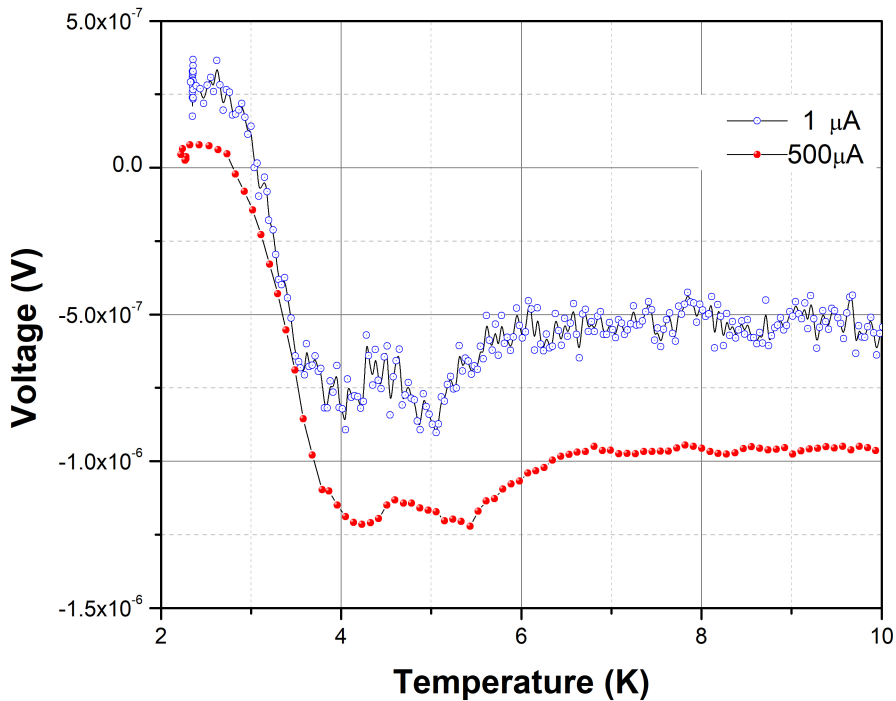


FIGURE 5.2: Variation of voltage for a range of temperature ($\approx 2\text{ K}$ to 10 K at constant currents $1\text{ }\mu\text{A}$ and $500\text{ }\mu\text{A}$).

On measuring the voltage for a range of temperature (from 2 K to 10 K) at a constant temperature of $1\text{ }\mu\text{A}$, we see significant noise in fig. 5.2 with no particular behaviour. However, doing the same experimental run for a current of $500\text{ }\mu\text{A}$, we observe a better plot as compared to the case of $1\text{ }\mu\text{A}$. However, even this plot does not yield any inferable data.

To check if the poor accuracy in plot 5.2 is due to stray background potential, we measure it at $0.3\text{ }\mu\text{A}$, and observe that the variation in voltage in fig. 5.3 shows no correspondence with plot 5.2.

On varying the input current from -2 mA to $+2\text{ mA}$ at a temperature of 2 K, we observe that there is a random variation of non-local voltage measurement in fig. 5.4 for a finite number of runs of the experiment. This as well, yields no inferable data.

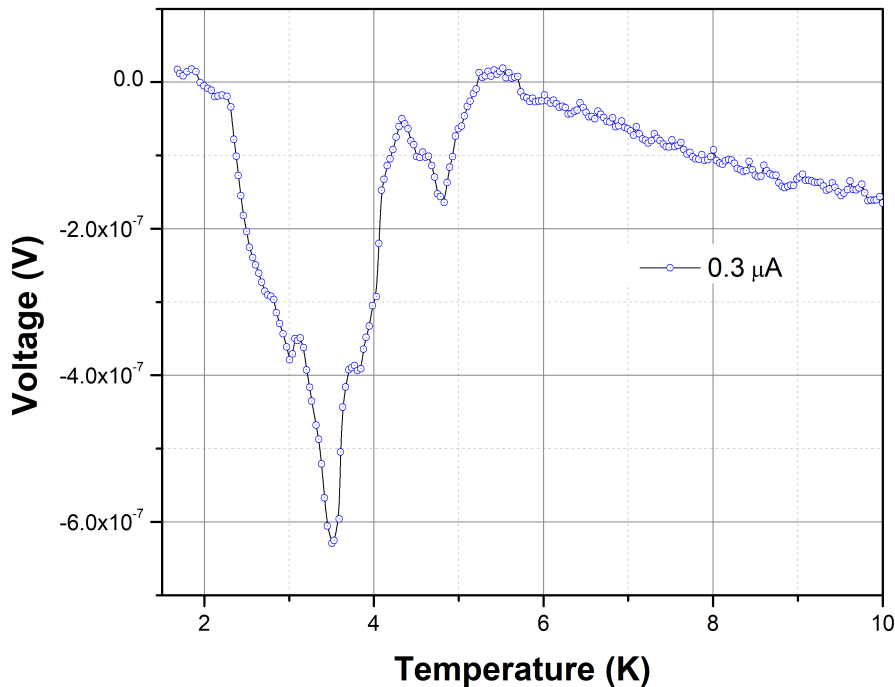


FIGURE 5.3: Testing voltage as a function of temperature against background.

5.0.1 Measurement via extrapolation in the presence of external B field

As suggested in section 4.3, we expected to observe a predictable pattern which could then be extrapolated to find the intercept on the y -axis (voltage measurement). However, a very noisy data was observed with no scope for extrapolation (see fig. 5.5).

5.0.2 Inference

We notice that no significant deviation from the above measurement data is seen when varying the length of the arm-link of the H-structure, as long as the length is within the spin diffusion length of Cu.

At varying thickness of the layers, as predicted in section 6.2.4 and eq. (4.8), we observe a better signal strength at a thickness of 10 nm, as compared to thicker slabs.

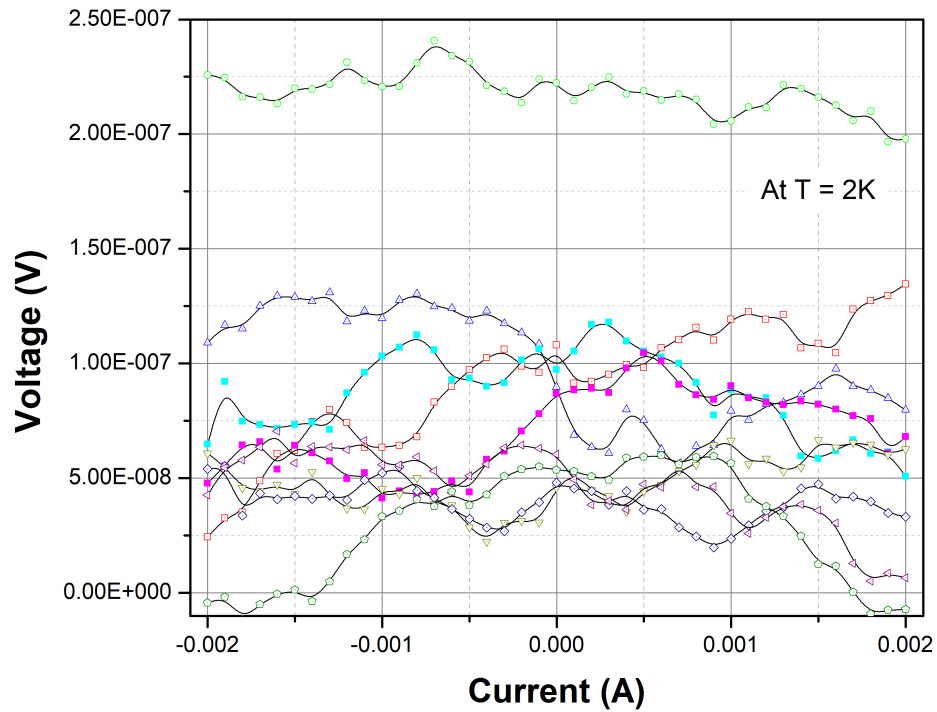


FIGURE 5.4: At $T = 2$ K, variation of potential difference as input current is varied from -2 mA to +2 mA for a finite number of runs.

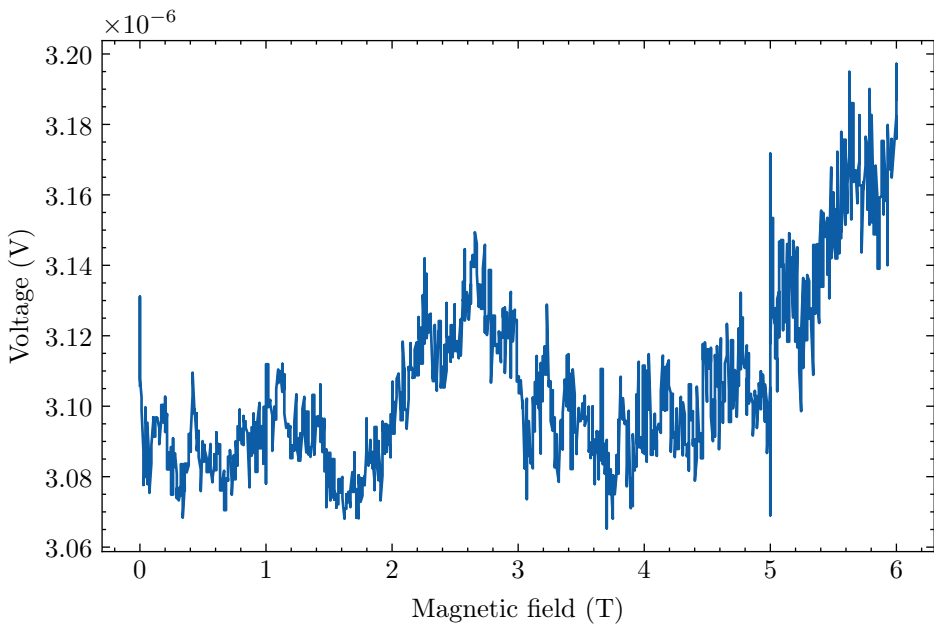


FIGURE 5.5: Plot of voltage V vs external magnetic field B , in presence of an external magnetic field

Chapter 6

Limitations & future prospects

6.1 Conclusion

The actual spin current reading is significantly low, upto the point that it gets hidden under background noise (in the form of stray potentials). Hence from an experimental point of view, we do not observe any meaningful correlation between the charge current in Pt and observed voltage measurement (see chapter 5).

6.2 Limitations

6.2.1 Generation of spin imbalance in Pt

We refer back to fig. 4.5, through which we evaluate the setup for reasons of low measurement readings (noisy) and proceed to suggest a better setup for measuring with greater efficacy in our next experimental run.

As seen in the figure, when J_c is passed through the first arm of the H-structure, a major portion of the current flows through Cu, it being an excellent conductor. This is however, not desirable since the generation of spin imbalance occurs due to Pt (because of its high SOC) and with the current setup, the amount of spin imbalance is reduced.

In an ideal setup, we would require most of the current to move through Pt, generating a "good" quantity of spin imbalance. The corresponding spin polarized electrons would then travel through the Cu layer, via the link and convert back to charge current.

6.2.2 Poor conversion efficiency

We mentioned earlier in section 4.4.1, that as opposed to typical experimental studies involving spin current detection which only involves a one-way conversion to charge current, we proceed to supply a charge current, followed by conversion to spin current, which is again followed by conversion to charge current, leading to a two-way conversion pathway.

Each time such a conversion occurs, the efficiency is poor (even if Pt has good SOC), leading to a poor measurement data for detecting spin current. This low measurement is further diminished in our setup, since we go through a two-way conversion pathway.

6.2.3 Complications with multilayered systems

Multilayered samples have the issue of current moving disproportionately amongst layers as opposed to the desired quantity for a good measurement. These complications arise due to movement of current through the interface of two materials (this might cause some dissipation) or due to shunting (which happens in our sample, due to both the materials being metals), which is undesirable and causes poor efficacy in measurement of spin current [33].

Ideally, one would like to use one material, which has good SOC to facilitate the conversion to spin current and good spin diffusion length δ_s , onto which both generation and detection can be done.

6.2.4 Thickness of layer

Using a thicker layer in our sample introduces a reduction in the current density along with an increase in resistance against current. We strongly try to avoid the former, since a greater current density yields a greater spin imbalance via SHE and consequently, voltage reading that can be accurately measured. This can be seen via eq. (4.8), where a thinner slab yields better spin Hall voltage.

6.3 Scope for improvement

As mentioned in sections 6.2.3 and 6.2.4, during the next run of the experiment, we aim to use a bilayer instead of a trilayer, hence reducing the number of NM-HM metal interfaces by one.

Also, the only purpose of the arm-link in the H-structure is to enable the flow of spin-polarized electrons in the form of spin current upto a greater distance, facilitated by the high spin diffusion length of Cu. Therefore, the support outer layers of Pt can be removed to concentrate all the spin current to flow through the middle layer of Cu.

6.4 Future prospects

Spintronics has a wide potential for drastically changing the technological industry for the better. As seen in chapter 1, Moore's law poses an alarming threat to conventional electronics and the technological sphere as we know it [3]. This upcoming field based on the spin of the electronic can be seen to have a vast potential in improving this dire situation and help produce devices much better in terms of power consumption and switching times [5].

Our study gives us a glimpse at the practical difficulties involved in making performant spin-based devices. For example, making transistors that work on spin is challenging as generation and detection of spin current is not very trivial [6].

Bibliography

- [1] C. Stamm et al. “Magneto-Optical Detection of the Spin Hall Effect in Pt and W Thin Films”. In: *Physical Review Letters* 119.8 (Aug. 2017). DOI: [10.1103/physrevlett.119.087203](https://doi.org/10.1103/physrevlett.119.087203). URL: <https://doi.org/10.1103/2Fphysrevlett.119.087203>.
- [2] SO Valenzuela and M Tinkham. “Electrical detection of spin currents: The spin-current induced Hall effect”. In: *Journal of applied physics* 101.9 (2007), 09B103.
- [3] Gordon E Moore. “Cramming more components onto integrated circuits”. In: *Proceedings of the IEEE* 86.1 (1998), pp. 82–85.
- [4] Saad Mabrouk Yakout. “Spintronics: Future Technology for New Data Storage and Communication Devices”. In: *Journal of Superconductivity and Novel Magnetism* 33.9 (May 2020), pp. 2557–2580. DOI: [10.1007/s10948-020-05545-8](https://doi.org/10.1007/s10948-020-05545-8). URL: <https://doi.org/10.1007%2Fs10948-020-05545-8>.
- [5] SA Wolf et al. “Spintronics: a spin-based electronics vision for the future”. In: *science* 294.5546 (2001), pp. 1488–1495.
- [6] Igor Žutić, Jaroslav Fabian, and S Das Sarma. “Spintronics: Fundamentals and applications”. In: *Reviews of modern physics* 76.2 (2004), p. 323.
- [7] A. S. “On a new Action of the Magnet on Electric Currents1”. In: *Nature* 21.537 (Feb. 1880), pp. 361–361. ISSN: 1476-4687. DOI: [10.1038/021361a0](https://doi.org/10.1038/021361a0). URL: <https://doi.org/10.1038/021361a0>.
- [8] Neil W Ashcroft, N David Mermin, et al. *Solid state physics*. Vol. 2005. holt, rinehart and winston, new york London, 1976.
- [9] Colin Hurd. *The Hall effect in metals and alloys*. Springer Science & Business Media, 2012.
- [10] JE Hirsch. “Spin hall effect”. In: *Physical review letters* 83.9 (1999), p. 1834.
- [11] Mikhail I Dyakonov and VI Perel. “Current-induced spin orientation of electrons in semiconductors”. In: *Physics Letters A* 35.6 (1971), pp. 459–460.
- [12] Kannan M Krishnan. *Fundamentals and applications of magnetic materials*. Oxford University Press, 2016.
- [13] John David Jackson. *Classical electrodynamics*. 1999.

- [14] Ken-ichi Uchida and Eiji Saitoh. “Spin Current”. In: *Spintronics for Next Generation Innovative Devices*. John Wiley & Sons, Ltd, Jan. 2016, pp. 43–76. DOI: [10.1002/9781118751886.ch3](https://doi.org/10.1002/9781118751886.ch3). URL: <https://doi.org/10.1002%2F9781118751886.ch3>.
- [15] Mikhail I D’Yakonov and VI Perel. “Possibility of orienting electron spins with current”. In: *Soviet Journal of Experimental and Theoretical Physics Letters* 13 (1971), p. 467.
- [16] Shuichi Murakami. “Spin Hall Effect and Inverse Spin Hall Effect”. In: *Spintronics for Next Generation Innovative Devices* (2015), pp. 77–98.
- [17] NF Mott and H Massey. *W 1965 The Theory of Atomic Collisions*. 1964.
- [18] G. Vignale. “Ten Years of Spin Hall Effect”. In: *Journal of Superconductivity and Novel Magnetism* 23.1 (Oct. 2009), pp. 3–10. DOI: [10.1007/s10948-009-0547-9](https://doi.org/10.1007/s10948-009-0547-9). URL: <https://doi.org/10.1007%2Fs10948-009-0547-9>.
- [19] Luc Berger. “Side-jump mechanism for the Hall effect of ferromagnets”. In: *Physical Review B* 2.11 (1970), p. 4559.
- [20] Axel Hoffmann. “Spin Hall effects in metals”. In: *IEEE transactions on magnetics* 49.10 (2013), pp. 5172–5193.
- [21] Jairo Sinova et al. “Universal intrinsic spin Hall effect”. In: *Physical review letters* 92.12 (2004), p. 126603.
- [22] Shufeng Zhang. “Spin Hall effect in the presence of spin diffusion”. In: *Physical review letters* 85.2 (2000), p. 393.
- [23] T Kimura et al. “Room-temperature reversible spin Hall effect”. In: *Physical review letters* 98.15 (2007), p. 156601.
- [24] Hongwei Li et al. “Spin-orbit torque-induced magnetization switching in epitaxial Au/Fe4N bilayer films”. In: *Applied Physics Letters* 114.9 (2019), p. 092402.
- [25] Christian Stamm et al. “Magneto-optical detection of the spin Hall effect in Pt and W thin films”. In: *Physical review letters* 119.8 (2017), p. 087203.
- [26] J-C Rojas-Sánchez et al. “Spin pumping and inverse spin Hall effect in platinum: the essential role of spin-memory loss at metallic interfaces”. In: *Physical review letters* 112.10 (2014), p. 106602.
- [27] Guang-Yu Guo et al. “Intrinsic spin Hall effect in platinum: First-principles calculations”. In: *Physical review letters* 100.9 (2008), p. 096401.
- [28] Luqiao Liu, RA Buhrman, and DC Ralph. “Review and analysis of measurements of the spin Hall effect in platinum”. In: *arXiv preprint arXiv:1111.3702* (2011).
- [29] O Gladii et al. “Spin wave amplification using the spin Hall effect in permalloy/ platinum bilayers”. In: *Applied Physics Letters* 108.20 (2016), p. 202407.
- [30] Rajagopalan Ramaswamy et al. “Extrinsic spin Hall effect in Cu 1- x Pt x”. In: *Physical Review Applied* 8.2 (2017), p. 024034.

- [31] RC Black et al. “Magnetic microscopy using a liquid nitrogen cooled YBa₂Cu₃O₇ superconducting quantum interference device”. In: *Applied physics letters* 62.17 (1993), pp. 2128–2130.
- [32] T. Kimura, J. Hamrle, and Y. Otani. “Estimation of spin-diffusion length from the magnitude of spin-current absorption: Multiterminal ferromagnetic /nonferromagnetic hybrid structures”. In: *Physical Review B* 72.1 (July 2005). DOI: [10.1103/physrevb.72.014461](https://doi.org/10.1103/physrevb.72.014461). URL: <https://doi.org/10.1103%2Fphysrevb.72.014461>.
- [33] Sadamichi Maekawa et al. *Spin current*. Vol. 22. Oxford University Press, 2017.